

Manipulating charge density wave state in kagome compound RbV_3Sb_5

Yu-Xin Meng(孟雨欣), Cheng-Long Xue(薛成龙), Li-Guo Dou(窦立国), Wei-Min Zhao(赵伟民), Qi-Wei Wang(汪琪玮), Yong-Jie Xu(徐永杰), Xiangqi Liu(刘祥麒), Wei Xia(夏威), Yanfeng Guo(郭艳峰), and Shao-Chun Li(李绍春)
Citation: Chin. Phys. B, 2023, 32 (**9**): 096801. DOI: 10.1088/1674-1056/acd8b1
Journal homepage: http://cpb.iphy.ac.cn; http://iopscience.iop.org/cpb

What follows is a list of articles you may be interested in

Critical behavior in the epitaxial growth of two-dimensional tellurium films on $SrTiO_3$ (001) substrates

Haimin Zhang(张海民), Dezhi Song(宋德志), Fuyang Huang(黄扶旸), Jun Zhang(仉君), and Ye-Ping Jiang(蒋烨平)
Chin. Phys. B, 2023, 32 (**6**): 066802. DOI: 10.1088/1674-1056/acc80d

Quasi-one-dimensional characters in topological semimetal $TaNiTe_5$

Ni Ma(马妮), De-Yang Wang(王德阳), Ben-Rui Huang(黄本锐), Kai-Yi Li(李凯仪), Jing-Peng Song(宋靖鹏), Jian-Zhong Liu(刘建忠), Hong-Ping Mei(梅红萍), Mao Ye(叶茂), and Ang Li(李昂)
Chin. Phys. B, 2023, 32 (**5**): 056801. DOI: 10.1088/1674-1056/aca203

Polarization Raman spectra of graphene nanoribbons

Wangwei Xu(许望伟), Shijie Sun(孙诗杰), Muzi Yang(杨慕紫), Zhenliang Hao(郝振亮), Lei Gao(高蕾), Jianchen Lu(卢建臣), Jiasen Zhu(朱嘉森), Jian Chen(陈建), and Jinming Cai(蔡金明)
Chin. Phys. B, 2023, 32 (**4**): 046803. DOI: 10.1088/1674-1056/ac80b3

Selective linear etching of monolayer black phosphorus using electron beams

Yuhao Pan(潘宇浩), Bao Lei(雷宝), Jingsi Qiao(乔婧思), Zhixin Hu(胡智鑫), Wu Zhou(周武), Wei Ji(季威)
Chin. Phys. B, 2020, 29 (**8**): 086801. DOI: 10.1088/1674-1056/ab9438

Tunable 2H-$TaSe_2$ room-temperature terahertz photodetector

Jin Wang(王瑾), Cheng Guo(郭程), Wanlong Guo(郭万龙), Lin Wang(王林), Wangzhou Shi(石旺舟), Xiaoshuang Chen(陈效双)
Chin. Phys. B, 2019, 28 (**4**): 046802. DOI: 10.1088/1674-1056/28/4/046802

Manipulating charge density wave state in kagome compound RbV_3Sb_5

Yu-Xin Meng(孟雨欣)[1,2], Cheng-Long Xue(薛成龙)[1,2], Li-Guo Dou(窦立国)[1,2], Wei-Min Zhao(赵伟民)[1,2], Qi-Wei Wang(汪琪玮)[1,2], Yong-Jie Xu(徐永杰)[1,2], Xiangqi Liu(刘祥麒)[3], Wei Xia(夏威)[3,4], Yanfeng Guo(郭艳峰)[3,4,†], and Shao-Chun Li(李绍春)[1,2,5,6,‡]

[1] *National Laboratory of Solid State Microstructures, School of Physics, Nanjing University, Nanjing* 210093, *China*
[2] *Collaborative Innovation Center of Advanced Microstructures, Nanjing University, Nanjing* 210093, *China*
[3] *School of Physical Science and Technology, Shanghai Tech University, Shanghai* 201210, *China*
[4] *Shanghai Tech Laboratory for Topological Physics, Shanghai* 201210, *China*
[5] *Jiangsu Provincial Key Laboratory for Nanotechnology, Nanjing University, Nanjing* 210093, *China*
[6] *Hefei National Laboratory, Hefei* 230088, *China*

(Received 17 April 2023; revised manuscript received 23 May 2023; accepted manuscript online 25 May 2023)

Owing to the unique electronic structure, kagome materials AV_3Sb_5 (A = K, Rb, Cs) provide a fertile platform of quantum phenomena such as the strongly correlated state and topological Dirac band. It is well known that RbV_3Sb_5 exhibits a 2×2 unconventional charge density wave (CDW) state at low temperature, and the mechanism is controversial. Here, by using scanning tunneling microscopy/spectroscopy (STM/STS), we successfully manipulated the CDW state in the Sb plane of RbV_3Sb_5, and realized a new $\sqrt{3}\times\sqrt{3}$ modulation together with the ubiquitous 2×2 period in the CDW state of RbV_3Sb_5. This work provides a new understanding of the collective quantum ground states in the kagome materials.

Keywords: kagome material, charge density wave, scanning tunneling microscopy

PACS: 68.37.Ef, 71.45.Lr, 73.20.At **DOI:** 10.1088/1674-1056/acd8b1

Kagome lattice is a corner-shared triangular network, and has attracted great attentions due to the intriguing electronic features including flat bands, Dirac cones and van Hove singularity (vHs). This model system exhibits various exotic properties, such as quantum spin liquid,[1,2] topological electronic states,[3–6] superconductivity (SC),[7–9] and charge density wave (CDW) states,[8–11] etc. Recently, a new family of kagome materials, namely AV_3Sb_5 (A = K, Rb, Cs), was discovered, in which rich quantum phases have been revealed.[12,13] AV_3Sb_5 undergoes both of the superconductivity transition (T_C =∼ 0.9 K–2.5 K) and the CDW (T_{CDW} =∼ 78 K–103 K).[12–14] During the CDW transition, an in-plane unit-cell doubling with the 2×2 periodicity[13,15–18] occurs, as also accompanied by a three-dimensional $2\times2\times2/2\times2\times4$ ordering[19,20] and a surface 1×4 superstructure.[15,21] It was considered that the CDW phase exhibits some complicated entanglement with the superconductivity transition.[22–24] The CDW electronic order was initially manifested in the transport measurement as a magnetic anomaly, and then explored through a myriad of experimental and theoretical methods.[16,25–32] Scanning tunneling microscopy/spectroscopy (STM/STS) studies reveled a chiral charge order in the three compounds with the 2×2 order,[33–35] and a rotational symmetry breaking of the electronic ground state from C_6 to C_2 at low temperatures.[36,37] This anisotropy was considered as a chiral charge order with broken time-reversal symmetry due to its magnetic field switching effect, and possibly related with the observed anomalous Hall effect without a magnetic order.[38,39] To unveil the driving force for the CDW transition is no doubt essential to the understanding of its interplay with the superconductivity and the kagome physics in AV_3Sb_5 materials. However, the mechanism of the CDW transition remains still under debate.

First-principle calculation and measurements indicated that the CDW transition is driven by the van Hove singularity-related Fermi surface (FS) nesting.[30,40] Angle-resolved photoelectron spectroscopy (ARPES) measurement demonstrated a substantial reconstruction of Fermi surface and the dominant role of the in-plane inter-saddle-point scattering to the CDW transition.[41] Optical characterization showed the importance of the saddle point nesting, in favor of the theoretical calculations as well.[26,29,42–44] Hard x-ray scattering revealed an unconventional CDW relevant to the kagome lattice nesting at vHs.[18] However, neutron scattering studies and other ARPES measurements indicated that the electron–phonon coupling plays a dominant role in generating the CDW phase.[45,46] In contrast, polarized Raman spectroscopic measurement did not show a phonon anomaly below and near the CDW transition temperature.[47] Even though quantum states with various pe-

†Corresponding author. E-mail: guoyf@shanghaitech.edu.cn
‡Corresponding author. E-mail: scli@nju.edu.cn

© 2023 Chinese Physical Society and IOP Publishing Ltd

riodic orders, such as spin charge density wave and charge bond wave, have been discussed in theoretical models, most of experimental studies have only reported the 2×2 order to date.[32,48–51]

In this study, by using scanning tunneling microscopy, we have characterized both of the Rb and Sb terminated planes in the RbV_3Sb_5 material. Via carefully tuning the tunneling condition and pulsing the surface, the surface Rb atoms were successfully removed and the underneath Sb layer is then *in-situ* exposed. We thus observed a new $\sqrt{3}\times\sqrt{3}$ modulation overlaid on the widely explored 2×2 CDW period. This $\sqrt{3}\times\sqrt{3}$ modulation is found to be less stable than the 2×2 one, and can be triggered by applying an STM pulse during scan on the 2×2 modulation.

The RbV_3Sb_5 single crystals were *in-situ* cleaved in ultra-high vacuum (UHV) at room temperature, and then immediately transfered into the STM stage for measurement. Scanning tunneling microscopy and spectroscopy (STM/STS) measurements were carried out at low-temperature of ~4.2 K or ~77 K in UHV, with the base pressure of 1×10^{-10} mbar (1 bar$=10^5$ Pa). STM topographic images were acquired under the constant current mode. Differential conductance $\mathrm{d}I/\mathrm{d}V$ spectra were obtained using the standard lock-in amplifier technique with an ac modulation of 10 mV at 1000 Hz.

RbV_3Sb_5 crystallizes in a hexagonal kagome lattice with the space group $P6/mmm$ ($a_0=5.47$ Å; $c_0=9.07$ Å), as schematically illustrated in Fig. 1(a). The two-dimensional (2D) kagome lattices are composed of V atoms coordinated by Sb atoms, which form interlayer V_3Sb lattices sandwiched by two layers of alkali metal ions. The 2×2 CDW transition occurs at ~103 K [14] and the superconductivity transition at ~0.9 K.[14]

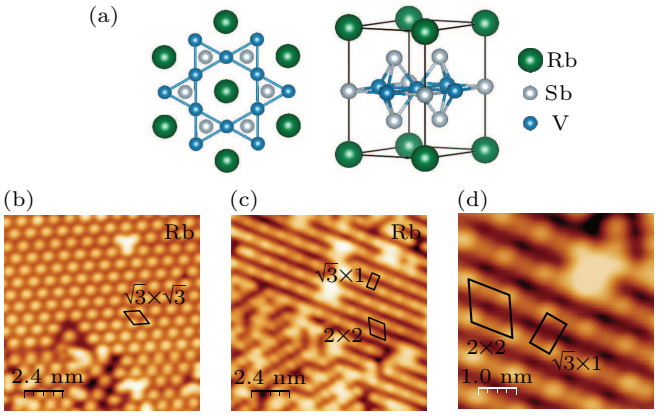


Fig. 1. (a) Crystal structure of RbV_3Sb_5 from top view (left) and 3D view (right). (b) STM topographic image (12 nm×12 nm) of the Rb-$\sqrt{3}\times\sqrt{3}$ terminated surface. $V_s=+500$ mV, $I_t=50$ pA. (c) STM topographic image (12 nm×12 nm) of the Rb-$\sqrt{3}\times1$ surface. $V_s=+50$ mV, $I_t=100$ pA. (d) A zoom-in STM image (5 nm×5 nm) of panel (c). $V_s=+50$ mV, $I_t=100$ pA.

Figures 1(b)–1(c) show the STM images collected on the as-cleaved surface of the RbV_3Sb_5 sample. Consistent with the previous studies,[52] most of the as-cleaved surface is covered by Rb atoms forming various superstructures. The Rb-$\sqrt{3}\times\sqrt{3}$ is the dominant superstructure with the Rb coverage of 1/3 monolayer (ML), as shown in Fig. 1(b). There also exists another $\sqrt{3}\times1$ superstructure mixed with a 2×2 modulation with the Rb coverage of 1/2 ML, as shown in Figs. 1(c) and 1(d). However, the 2×2 CDW period, that occurs in the underneath Sb or Sb–V kagome plane, is invisible in the Rb-$\sqrt{3}\times\sqrt{3}$ plane.

In order to directly envision the CDW modulation in the underneath Sb planes, we turned to *in-situ* remove the surface Rb atoms by applying high tunneling current and low bias voltage. Figure 2(a) shows a typical STM image collected on the pristine as-cleaved surface with a normal tunneling current and bias voltage. By increasing the tunneling current and lowering the bias voltage, the STM tip was pushed much closer to the surface to enhance the tip-surface coupling. The surface Rb atoms can be thus swiped away by STM tip during the scan with a high current and low bias voltage. In this way, the clean Sb plane underneath the Rb plane was successfully exposed without Rb atoms. Figures 2(a)–2(c) show the series of STM images collected at the same area during atom swiping. As shown in Fig. 2(c), the 2×2 modulation is clearly identified as the characteristic of the CDW phase, which is consistent with the previous studies.[13,15–18] The $\mathrm{d}I/\mathrm{d}V$ spectra taken on the Sb terminated plane is plotted in Fig. 2(d). According to the previous studies,[15,21] in the Sb plane spectrum we attribute the peaks at -400 mV and -150 mV to the van Hove singularity (vHs) of the electronic states at M point, and the local minimum near -600 mV is related to the Dirac point (DP) at K point. The V-shaped energy dip located near the Fermi level may correspond to the CDW gap, and is considered to be connected with the electronic states near the M point.[53] For comparison, the $\mathrm{d}I/\mathrm{d}V$ spectrum taken on the Rb terminated plane is also plotted in Fig. 2(d). The $\mathrm{d}I/\mathrm{d}V$ spectrum taken on the two terminations looks very similar except for an energy shift of ~130 mV, suggesting that upon removing the alkali layer, the Fermi energy is moved downward induced by an effective hole doping.[54]

Surprisingly, once the tunneling current and bias voltage were suddenly changed, an effective STM pulse was made via the tunneling instability, and we observed a new $\sqrt{3}\times\sqrt{3}$ modulation transformed from the original 2×2 one, as shown in the STM images of Figs. 2(e) and 2(f) and the corresponding fast Fourier transform (FFT). In order to make the results more accurate, the FFT images are derived from the defect-free region in STM images. The peaks of 2×2 order in three directions can be seen clearly in Fig. 2(e), both the first order and second order spots are denoted. While the spots of $\sqrt{3}\times\sqrt{3}$ modulation only appear in one direction in Fig. 2(f). It is manifested that the $\sqrt{3}$ times modulation coexists with the 2×2 order, and is most obvious in the horizontal direction. Unlike the original 2×2 modulation, the generated $\sqrt{3}\times\sqrt{3}$ modulation is only short-range ordered, and exists as the small patches of a few unit cells, as shown in Fig. 2(f). Therefore,

we suggest that, even though thermodynamically less stable than the 2×2 order, the formation of $\sqrt{3}\times\sqrt{3}$ modulation can be realized by a slight energy trigger, particularly through an STM pulse.

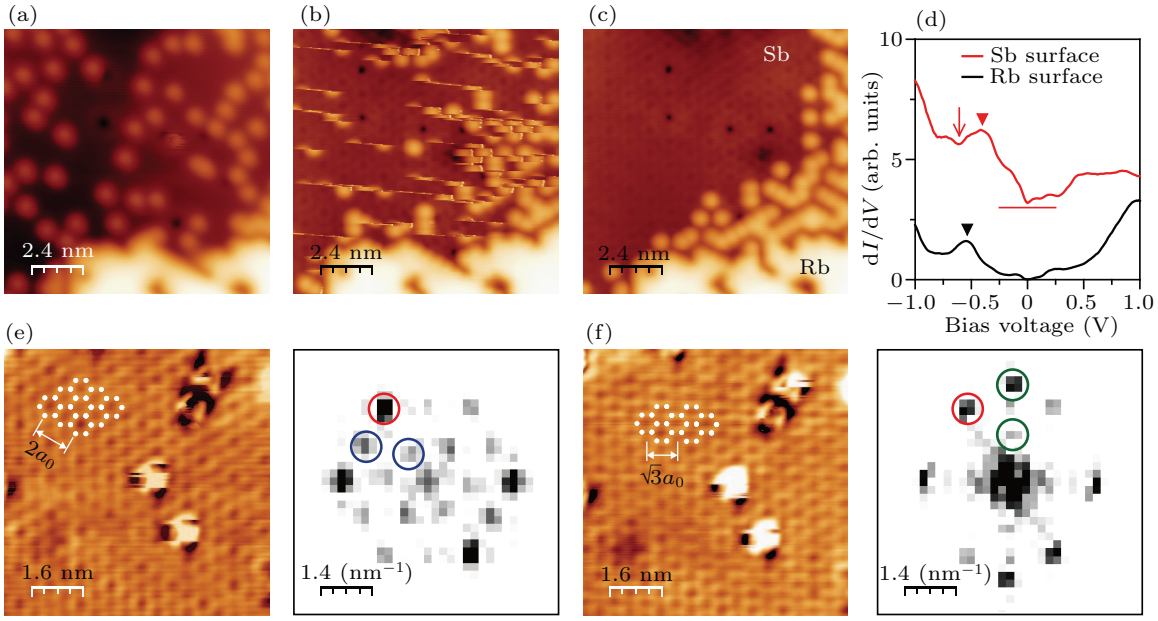


Fig. 2. (a)–(c) STM images (12 nm×12 nm) *in-situ* collected on the RbV_3Sb_3 surface during swiping surface Rb atoms by STM tip. (a) $V_s=-500$ mV, $I_t=-100$ pA; (b) $V_s=-80$ mV, $I_t=-100$ pA; (c) $V_s=-200$ mV, $I_t=-100$ pA. (d) Differential conductance dI/dV spectrum taken on the Rb (black) and Sb (red) terminated planes. The data are taken before and after removing the surface Rb atoms, respectively. The peaks of van Hove singularity in Rb and Sb planes are marked by black and red triangles, respectively. The local minimum is denoted by red arrow. The red curve is shifted upward by 3 for clarity. (e)–(f) Topographic images (10 nm×10 nm) of the Sb plane prior to and after the STM voltage pulses. $V_s=+80$ mV (e) and +120 mV (f), $I_t=100$ pA. The insets show the corresponding fast Fourier transform images of the defect-free region. The red, blue, and green circles mark the vectors of Bragg lattice, 2×2 and $\sqrt{3}\times\sqrt{3}$ modulations, respectively.

In order to further confirm the coexistence of 2×2 and $\sqrt{3}\times\sqrt{3}$ orders, we took the spatially-resolved dI/dV measurement along the line in Fig. 3(a). Along this particular direction, the $\sqrt{3}\times\sqrt{3}$ and 2×2 orders correspond to the three and two times modulations, respectively. In Fig. 3(b) are plotted the measured position-dependent dI/dV results, where the periods of both order are distinguishable. As marked in Fig. 3(b), the $\sqrt{3}\times\sqrt{3}$ order is prominent in the negative bias range, while the 2×2 order in the positive bias range. Two particular dI/dV densities, as extracted from the bias voltage (V_s) of -0.3 V and $+0.45$ V, are plotted in Fig. 3(c) for a better view of these two orders. The $\sqrt{3}\times\sqrt{3}$ order is marked by the green triangles on the red curve of $V_s=-0.3$ V, and the 2×2 order by the blue triangles on the black curve of $V_s=+0.45$ V. The FFT graphs of the two curves, as shown in Fig. 3(d), further confirm the existence of the $\sqrt{3}\times\sqrt{3}$ and 2×2 orders. Our observation indicates that the $\sqrt{3}\times\sqrt{3}$ order is likely less stable than the 2×2 one, and its formation can be triggered by an STM pulse applied on the 2×2 order.

It is well known that the saddle points of the Dirac bands are located at the M point in the Brillouin zone, closing to the Fermi level.[26,44] The vectors connecting the van Hove singularities at M points were believed to be responsible for the formation of 2×2 order, thus in favor of the Fermi surface nesting mechanism.[29,42] Moreover, the Kagome Hubbard model at van Hove filling, with the on-site repulsion U and the nearest-neighbor Coulomb interaction V, were also adopted to theoretically predict the electronic phases of kagome materials.[8,55–58] Within this theoretical model, the adopted Fermi surface and vHs, as schematically illustrated in Fig. 4(a), is consistent with the experimental results.[26,27,29,32,50] The Bloch states connected by the nesting vectors are distributed among the three diverse sublattices, as illustrated in Fig. 4(b).[7–9] The nearest-neighbor interaction V is found to lead to a different electron density on the neighboring lattice sites. As V is promoted, the 2×2 modulation firstly appears. Since the nesting vector connects the electronic states of different sublattices, each sublattice hosts a uniform electron density.[28,32] However, as V is increased to a larger value, electrons tend to accumulate in fewer sites, and the electron intensity does not need to remain uniform at the different sublattices. Thus the 2×2 modulation turns to a $\sqrt{3}\times\sqrt{3}$ modulation as a consequence to reduce the nesting effects for a local Hubbard interaction.

Even though the physical nature that drives the formation of $\sqrt{3}\times\sqrt{3}$ modulation is still unknown, we believe it is possibly due to a tip-induced local deformation that tunes the nearest-neighbor interaction V, or a local doping effect that shifts the position of vHs. According to the previous theoretical work, our observation of both the $\sqrt{3}\times\sqrt{3}$ and 2×2 orders may suggest that the nearest-neighbor interaction V is important to lead to the rich CDW ground states, via tuning

the electronic states of the sub-lattices. The emergence of the $\sqrt{3}\times\sqrt{3}$ modulation may be also related to the removing of the upper Rb atoms, the deficiency of Rb atoms can affect the electronic states of the lower Sb layer. For instance, to remove the Rb plane can induce an effective hole doping and shift the Fermi level downward by ~ 130 mV, as demonstrated in Fig. 2(d). The vHs can be thus shifted away from the M points, which weakens the Fermi surface nesting effect.

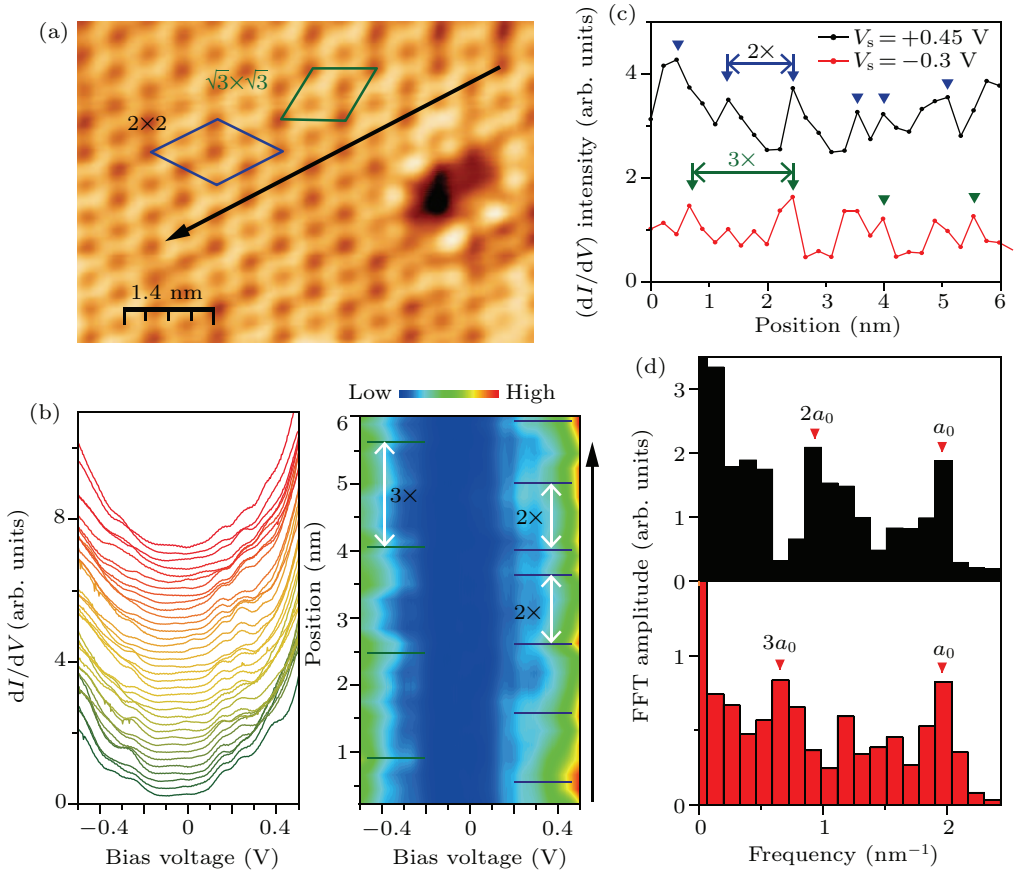


Fig. 3. (a) Topographic image (6.8 nm×4.8 nm) taken on the Sb plane of the RbV_3Sb_5 sample. $V_s = -200$ mV, $I_t = -150$ pA. (b) Line-scan dI/dV spectra taken along the symmetric direction as marked by the black arrowed line in panel (a). (c) Spatial variation of the dI/dV intensity extracted at +0.45 V and −0.3 V from the spectra in panel (b). The blue and green triangles mark the 2×2 and $\sqrt{3}\times\sqrt{3}$ modulations, respectively. The black curve is shifted upward by 1 for clarity. (d) The FFT graphs of the two line scan profile in panel (c) with corresponding color. The peaks of two modulations are denoted by red triangles.

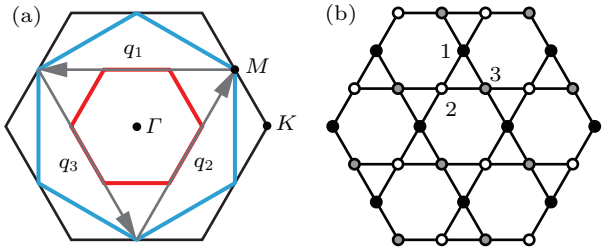


Fig. 4. (a) Momentum-space illustration of the kagome AV_3Sb_5. The outer black hexagon is the original Brillouin zone, the middle blue one the schematic Fermi surface, and the inner red one the new Brillouin zone under 2×2 modulation. The high symmetry points are marked as Γ, M, and K. The nesting wave vectors are illustrated by the three black arrowed lines as marked by q_1, q_2, and q_3. (b) Real-space illustration of the atomic structure in the kagome lattice. The labels 1 to 3 denote the three different sublattices.

In summary, we observed a $\sqrt{3}\times\sqrt{3}$ modulation in addition to the ubiquitous 2×2 CDW in RbV_3Sb_5. According to the previous kagome Hubbard model with extended Coulomb interactions, the two modulations are tunable via the electron states within the sublattices.[28,32] The transformation from 2×2 to $\sqrt{3}\times\sqrt{3}$ modulation is possibly caused by the reduced Fermi surface nesting or a variable local nearest-neighbor Coulomb interaction.

Acknowledgements

Project supported by the National Key Research and Development Program of China (Grant No. 2021YFA1400403), the National Natural Science Foundation of China (Grant Nos. 92165205, 11790311, and 11774149), and Innovation Program for Quantum Science and Technology (Grant No. 2021ZD0302800). Y F Guo acknowledges the support by the open project of Beijing National Laboratory for Condensed Matter Physics (Grant No. ZBJ2106110017) and the Double First-Class Initiative Fund of Shanghai Tech University.

References

[1] Balents L 2010 *Nature* **464** 199
[2] Simeng Yan D A H and Steven R White 2011 *Science* **332** 1173
[3] Guo H M and Franz M 2009 *Phys. Rev. B* **80** 113102

[4] Kang M, Ye L, Fang S, You J S, Levitan A, Han M, Facio J I, Jozwiak C, Bostwick A, Rotenberg E, Chan M K, McDonald R D, Graf D, Kaznatcheev K, Vescovo E, Bell D C, Kaxiras E, van den Brink J, Richter M, Prasad Ghimire M, Checkelsky J G and Comin R 2020 *Nat. Mater.* **19** 163

[5] Wang Q, Xu Y, Lou R, Liu Z, Li M, Huang Y, Shen D, Weng H, Wang S and Lei H 2018 *Nat. Commun.* **9** 3681

[6] Yin J X, Zhang S S, Chang G, Wang Q, Tsirkin S S, Guguchia Z, Lian B, Zhou H, Jiang K, Belopolski I, Shumiya N, Multer D, Litskevich M, Cochran T A, Lin H, Wang Z, Neupert T, Jia S, Lei H and Hasan M Z 2019 *Nat. Phys.* **15** 443

[7] Yu S L and Li J X 2012 *Phys. Rev. B* **85** 144402

[8] Kiesel M L, Platt C and Thomale R 2013 *Phys. Rev. Lett.* **110** 126405

[9] Kiesel M L and Thomale R 2012 *Phys. Rev. B* **86** 121105

[10] Wang W S, Li Z Z, Xiang Y Y and Wang Q H 2013 *Phys. Rev. B* **87** 115135

[11] Ye L, Kang M, Liu J, von Cube F, Wicker C R, Suzuki T, Jozwiak C, Bostwick A, Rotenberg E, Bell D C, Fu L, Comin R and Checkelsky J G 2018 *Nature* **555** 638

[12] Ortiz B R, Gomes L C, Morey J R, Winiarski M, Bordelon M, Mangum J S, Oswald L W H, Rodriguez-Rivera J A, Neilson J R, Wilson S D, Ertekin E, McQueen T M and Toberer E S 2019 *Phys. Rev. Mater.* **3** 094407

[13] Ortiz B R, Teicher S M L, Hu Y, Zuo J L, Sarte P M, Schueller E C, Abeykoon A M M, Krogstad M J, Rosenkranz S, Osborn R, Seshadri R, Balents L, He J F and Wilson S D 2020 *Phys. Rev. Lett.* **125** 247002

[14] Yin Q W, Tu Z J, Gong C S, Fu Y, Yan S H and Lei H C 2021 *Chin. Phys. Lett.* **38** 037403

[15] Zhao H, Li H, Ortiz B R, Teicher S M L, Park T, Ye M X, Wang Z Q, Balents L, Wilson S D and Zeljkovic I 2021 *Nature* **599** 216

[16] Jiang Y X, Yin J X, Denner M M, Shumiya N, Ortiz B R, Xu G, Guguchia Z, He J, Hossain M S, Liu X, Ruff J, Kautzsch L, Zhang S S, Chang G, Belopolski I, Zhang Q, Cochran T A, Multer D, Litskevich M, Cheng Z J, Yang X P, Wang Z, Thomale R, Neupert T, Wilson S D and Hasan M Z 2021 *Nat. Mater.* **20** 1353

[17] Bai X C, Wu W F, Wang H Y, Quan Y M, Wang X, Zeng Z and Zou L J 2022 *New J. Phys.* **24** 123016

[18] Li H, Zhang T T, Yilmaz T, Pai Y Y, Marvinney C E, Said A, Yin Q W, Gong C S, Tu Z J, Vescovo E, Nelson C S, Moore R G, Murakami S, Lei H C, Lee H N, Lawrie B J and Miao H 2021 *Phys. Rev. X* **11** 031050

[19] Liang Z W, Hou X Y, Zhang F, Ma W R, Wu P, Zhang Z Y, Yu F H, Ying J J, Jiang K, Shan L, Wang Z Y and Chen X H 2021 *Phys. Rev. X* **11** 031026

[20] Ortiz B R, Teicher S M L, Kautzsch L, Sarte P M, Ratcliff N, Harter J, Ruff J P C, Seshadri R and Wilson S D 2021 *Phys. Rev. X* **11** 041030

[21] Chen H, Yang H T, Hu B, Zhao Z, Yuan J, Xing Y Q, Qian G J, Huang Z H, Li G, Ye Y H, Ma S, Ni S L, Zhang H, Yin Q W, Gong C S, Tu Z J, Lei H C, Tan H X, Zhou S, Shen C M, Dong X L, Yan B H, Wang Z Q and Gao H J 2021 *Nature* **599** 222

[22] Song Y, Ying T, Chen X, Han X, Wu X, Schnyder A P, Huang Y, Guo J G and Chen X 2021 *Phys. Rev. Lett.* **127** 237001

[23] Qian T, Christensen M H, Hu C W, Saha A, Andersen B M, Fernandes R M, Birol T and Ni N 2021 *Phys. Rev. B* **104** 144506

[24] Yu F H, Ma D H, Zhuo W Z, Liu S Q, Wen X K, Lei B, Ying J J and Chen X H 2021 *Nat. Commun.* **12** 3645

[25] Wang Q, Kong P, Shi W, Pei C, Wen C, Gao L, Zhao Y, Yin Q, Wu Y and Li G 2021 *Adv. Mater.* **33** 2102813

[26] Denner M M, Thomale R and Neupert T 2021 *Phys. Rev. Lett.* **127** 217601

[27] Lin Y P and Nandkishore R M 2021 *Phys. Rev. B* **104** 045122

[28] Wang C, Liu S, Jeon H and Cho J H 2022 *Phys. Rev. B* **105** 045135

[29] Neupert T, Denner M M, Yin J X, Thomale R and Hasan M Z 2022 *Nat. Phys.* **18** 137

[30] Kang M, Fang S, Kim J K, Ortiz B R, Ryu S H, Kim J, Yoo J, Sangiovanni G, Di Sante D, Park B G, Jozwiak C, Bostwick A, Rotenberg E, Kaxiras E, Wilson S D, Park J H and Comin R 2022 *Nat. Phys.* **18** 301

[31] Wu S, Ortiz B R, Tan H, Wilson S D, Yan B, Birol T and Blumberg G 2022 *Phys. Rev. B* **105** 155106

[32] Ferrari F, Becca F and Valentí R 2022 *Phys. Rev. B* **106** L081107

[33] Feng X, Jiang K, Wang Z and Hu J 2021 *Sci. Bull.* **66** 1384

[34] Wang Z W, Jiang Y X, Yin J X, Li Y K, Wang G Y, Huang H L, Shao S, Liu J J, Zhu P, Shumiya N, Hossain M S, Liu H X, Shi Y G, Duan J X, Li X, Chang G Q, Dai P C, Ye Z J, Xu G, Wang Y C, Zheng H, Jia J F, Hasan M Z and Yao Y G 2021 *Phys. Rev. B* **104** 075148

[35] Shumiya N, Hossain M S, Yin J X, Jiang Y X, Ortiz B R, Liu H X, Shi Y G, Yin Q W, Le H C, Zhan S T, Chang G Q, Zhang Q, Cochran T A, Multer D, Litskevich M, Cheng Z J, Yang X, Guguchia Z, Wilson S D and Hasan M Z 2021 *Phys. Rev. B* **104** 035131

[36] Nie L, Sun K, Ma W, Song D, Zheng L, Liang Z, Wu P, Yu F, Li J, Shan M, Zhao D, Li S, Kang B, Wu Z, Zhou Y, Liu K, Xiang Z, Ying J, Wang Z, Wu T and Chen X 2022 *Nature* **604** 59

[37] Li H, Zhao H, Ortiz B R, Park T, Ye M, Balents L, Wang Z, Wilson S D and Zeljkovic I 2022 *Nat. Phys.* **18** 265

[38] Yu F H, Wu T, Wang Z Y, Lei B, Zhuo W Z, Ying J J and Chen X H 2021 *Phys. Rev. B* **104** L041103

[39] Yang S Y, Wang Y J, Ortiz B R, Liu D F, Gayles J, Derunova E, Gonzalez-Hernandez R, Smejkal L, Chen Y L, Parkin S S P, Wilson S D, Toberer E S, McQueen T and Ali M N 2020 *Sci. Adv.* **6** eabb6003

[40] Cho S, Ma H, Xia W, Yang Y, Liu Z, Huang Z, Jiang Z, Lu X, Liu J, Liu Z, Li J, Wang J, Liu Y, Jia J, Guo Y, Liu J and Shen D 2021 *Phys. Rev. Lett.* **127** 236401

[41] Kato T, Li Y, Kawakami T, Liu M, Nakayama K, Wang Z, Moriya A, Tanaka K, Takahashi T, Yao Y and Sato T 2022 *Commun. Mater.* **3** 30

[42] Zhou X X, Li Y K, Fan X W, Hao J H, Dai Y M, Wang Z W, Yao Y G and Wen H H 2021 *Phys. Rev. B* **104** L041101

[43] Lou R, Fedorov A, Yin Q, Kuibarov A, Tu Z, Gong C, Schwier E F, Buchner B, Lei H and Borisenko S 2022 *Phys. Rev. Lett.* **128** 036402

[44] Tan H, Liu Y, Wang Z and Yan B 2021 *Phys. Rev. Lett.* **127** 046401

[45] Xie Y, Li Y, Bourges P, Ivanov A, Ye Z, Yin J X, Hasan M Z, Luo A, Yao Y, Wang Z, Xu G and Dai P 2022 *Phys. Rev. B* **105** L140501

[46] Luo H, Gao Q, Liu H, Gu Y, Wu D, Yi C, Jia J, Wu S, Luo X, Xu Y, Zhao L, Wang Q, Mao H, Liu G, Zhu Z, Shi Y, Jiang K, Hu J, Xu Z and Zhou X J 2022 *Nat. Commun.* **13** 273

[47] Wulferding D, Lee S, Choi Y, Yin Q, Tu Z, Gong C, Lei H, Yousuf S, Song J, Lee H, Park T and Choi K Y 2022 *Phys. Rev. Res.* **4** 023215

[48] Mertz T, Wunderlich P, Bhattacharyya S, Ferrari F and Valentí R 2022 *npj Comput. Mater.* **8** 66

[49] Feng X, Zhang Y, Jiang K and Hu J 2021 *Phys. Rev. B* **104** 165136

[50] Park T, Ye M and Balents L 2021 *Phys. Rev. B* **104** 035142

[51] Ferhat K and Ralko A 2014 *Phys. Rev. B* **89** 155141

[52] Yu J, Xu Z, Xiao K, Yuan Y, Yin Q, Hu Z, Gong C, Guo Y, Tu Z, Tang P, Lei H, Xue Q K and Li W 2022 *Nano Lett.* **22** 918

[53] Wang Z, Ma S, Zhang Y, Yang H, Zhao Z, Ou Y, Zhu Y, Ni S, Lu Z, Chen H, Jiang K, Yu L, Zhang Y, Dong X, Hu J, Gao H J and Zhao Z 2021 arXiv: 2104.05556v1

[54] Li Q Y, Lv Y Y, Xu Y J, Zhu L, Zhao W M, Chen Y and Li S C 2022 *Chin. Phys. B* **31** 066802

[55] Wen J, Rüegg A, Wang C C J and Fiete G A 2010 *Phys. Rev. B* **82** 075125

[56] Rüegg A and Fiete G A 2011 *Phys. Rev. B* **83** 165118

[57] O'Brien A, Pollmann F and Fulde P 2010 *Phys. Rev. B* **81** 235115

[58] Nishimoto S, Nakamura M, O'Brien A and Fulde P 2010 *Phys. Rev. Lett.* **104** 196401